SEMARAK ILMU PUBLISHING

CFD Letters

Journal homepage:
https://semarakilmu.com.my/journals/index.php/CFD_Letters/index
ISSN: 2180-1363

Diffusion of a Surface Marine Sewage Effluent

Sahameddin Mahmoudi Kurdistani [1,*], Gianluca Cosimo Perrone[1]

[1] IA.ING Engineering, Viale M. Chiatante, 60 - 73100 Lecce, Italy

ARTICLE INFO

Article history:
Received 14 May 2023
Received in revised form 18 June 2023
Accepted 10 July 2023
Available online 1 December 2023

Keywords:
Marine Surface Discharges; Scalar Intrusion Length; CFD; RANS; Numerical Modelling; Two Phase Flow

ABSTRACT

Any scalar concentration discharging to the sea through a freshwater release is a thermodynamic two-phase flow including different densities and different temperatures. Because of Reynolds similarity, physical models are not feasible to use and numerical models such as CFD-RANS are the solutions. A series of numerical experiments have been conducted to derive an empirical formula that determines the length of the 95% scalar concentration reduction, useful for primary and emergency engineering-environmental decisions. Results show that the scalar concentration intrusion length is a function of seawater density-temperature, freshwater density-temperature, sea current Froude number, effluent jet Froude number, and the scalar concentration in which among those, the sea current Froude number has the most effective role in which as an example of the lowest and highest tested sea current velocities, an effluent discharge of 0.052 m^3/s with a concentration of 1 Kg/m^3 and effluent jet velocity 0.245 m/s in 3.2 meters from the effluent source reaches to the 95% scalar concentration reduction when there is a high-velocity sea current (0.5 m/s) while in the presence of a low-velocity sea current (0.05 m/s), the same effluent discharge with the same scalar concentration and the same effluent jet velocity, the length of the 95% scalar concentration reduction increase to 42.8 meters from the effluent source.

1. Introduction

When sewage is discharged into the sea, the kinetic energy of the jet is dissipated in its surrounding seawater, and due to the interaction of the turbulence of the discharged jet and the natural turbulence in the ocean, the discharged sewage will lose its primary concentration in which after the initial jet-mixing, the sewage flows gently with the ocean as if it was part of it [1]. Among others, Chow *et al.,* [2], Kim *et al.,* [3], Bricker, *et al.,* [4], Zhao, *et al.,* [5], Inan, *et al.,* [6], Wang *et al.,* [7], Ho *et al.,* [8], Panseriya *et al.,* [9], and Santavy *et al.,* [10] gave important contributions to investigate the marine outfall sewage effluent dispersion phenomenon.

A literature review resulted in a limited number of scientific contributions on surface marine sewage effluent diffusion. Brooks [11] analyzed the lateral mixing of a sewage field in an ocean current taking into account the increasing eddy diffusivity as the field spreads. He derived the exact

* *Corresponding author.*
E-mail address: kurdistani@iaing.it (Sahameddin Mahmoudi Kurdistani)

https://doi.org/10.37934/cfdl.15.12.135153

solution of the partial differential equation balancing diffusion-advection, and mortality of coliform bacteria, in which the concentration was a function of the position in the horizontal plane downstream of the ideal line source. He presented three expressions for the rate of spread of a sewage field and for concentrations along the centreline of the field downstream of the source without presenting any explicit equations to determine the maximum length of the 95% scalar concentration reduction.

Bennett [12] conducting a series of field measurements showed that the fundamental mechanisms governing dilution in a sea current have a different effect from those conditions set up and measured in a laboratory under still water conditions. He found an additional diluting effect coming from the complex influence of the sea current on the emerging sewage plume. He proposed a formula for general application in comparable non-stratified moving water environments with the lack of presenting an expression for the length of the maximum dilution. Sharp [13] showed that consideration of ocean outfalls should be dealt with on an individual basis, taking into account the effluent and receiving water conditions. The effect of the sea-current condition has been highlighted by Caine [14]; he showed that the nature of the receiving water will dictate the extent of treatment, combined with the outfall location, that is necessary to achieve a sustainable system.

Matos *et al.,* [15] conducted a mathematical model for the "Costa do Estoril" outfall system and by means of the results from the mathematical model along with the field observations showed that the complexity of discharged sewage dilution derives from the fact that the sea currents are usually neither steady nor uniform and the plumes from two different diffusers may merge together, depending on the wastewater flow and density profiles.

Montaño-Ley *et al.,* [16] applied a vertically integrated semi-implicit, non-linear, finite difference model, to investigate the Urias Coastal Lagoon (UCL) hydrodynamics and pollutant dispersion focusing on the effect of the current velocity during ebb tide on the pollutant diffusion. Their numerical simulation of pollutant dispersion indicates that differentially higher ebb velocities have the effect of flushing pollutants.

Marques *et al.,* [17] developed a new algorithm for applying horizontal eddy diffusion within the surface boundary layer of general vertical coordinate system ocean models; using re-gridding/remapping techniques to represent tracer profiles in a geopotential vertical coordinate, where horizontal fluxes are easily calculated and then remapped back to the native grid.

The closest contribution to the current study was from Kim and Cho [18] that calibrated a CFD-RANS model (Flow-3D) and verified the accuracy of the numerical results using the hydraulic experimental data adapted from McGurik and Rodi [19]. They numerically studied the buoyant flow and mixing characteristics of heated water discharged from the surface and submerged side outfalls in shallow and deep water considering the effect of the sewage jet Froude numbers and the sea current Froude numbers. They showed that in shallow water, the submerged discharge has a higher minimum dilution than the surface discharge because of the more active initial mixing. They did not present any expression to determine the length of the maximum dilution.

As it appears from the literature review, in the previous studies, there is a gap in presenting an empirical formula to predict the scalar intrusion length inside the sea at surface marine discharges. Because of Reynolds similarity, making a laboratory experimental study is not feasible and numerical models such as CFD-RANS are the solutions. The current study aims to present an explicit formula to determine the length of the 95% scalar concentration reduction using the results from a series of numerical experiments. In particular, the interaction of sewage discharge and the sea current has been investigated. The procedure described herein is not applicable to tidal estuaries because they are limited in lateral extent and it needs to determine the longitudinal scalar intrusion length accompanying tidal motions and river flow.

2. Methodology

2.1 Numerical Modeling

The numerical modeling of a marine drain usually includes the analysis of hydrodynamic and water quality components. Hydrodynamic models are based on the principles of conservation of mass and momentum while water quality models are based on considerations relating to the mass of contaminants or tracers discharged. Hydrodynamic models are generally based on a fixed mesh in space (i.e., an Eulerian formulation) and produce the depth and velocity fields as an output. Water quality models require the velocity field as an input and their formulation can be based on the same mesh as the hydrodynamic model [20].

Another formulation is the Lagrangian formulation, where parcels of contaminant or tracer can be tracked while the velocity field transports and disperses them. The results of an Eulerian formulation produce the contaminant concentrations on the fixed network, while the Lagrangian formulation provides the number of contaminating particles contained in each volume of fluid delimited by mesh points or nodes: this enumeration can then be converted into contaminant concentration [20]. The numerical model to study the effluent dilution usually is composed of an appropriate turbulent model and a 3-D advection–diffusion model, specifically for coastal areas with important effects of wave stirring included [20].

2.2 CFD Model

Flow-3D from Flow Science Inc. is a readily-available, state-of-the-art CFD model which is used to define the quantities concerning fluid dynamics and tracking of the free surface, based on the Reynolds Averaged Navier-Stokes (RANS) equations, together with methods for defining turbulent stresses [21]. Flow-3D is widely used in industry i.e. BMW Group [22] and recently, has been employed to study the wave-induced pore pressure distribution inside the breakwater core by Vanneste and Troch [23], and Kurdistani *et al.,* [24, 25].

2.3 Reynolds Averaging and VOF Approach

All the calculations in the current study are based on the Reynolds-Averaged Navier-Stokes (RANS) approach [26]. Due to creating a numerical mesh using a VOF-RANS model for free surface tracking without investing time to create a new code, Flow-3D hydrodynamic model from Flow Science Inc. has been employed. The *volume-of-fluid* (VOF) approach [27, 28] presents the fraction F of the cell filled with fluid as $F = 0$ outside the fluid domain, $F = 1$ within the interior of the fluid, and $0 < F < 1$ for cells that are cut by a boundary. The general mass continuity equation using the fluid fraction can be written as:

$$\frac{\partial F}{\partial t} + \frac{\partial F u_i}{\partial x_i} = 0 \tag{1}$$

where the computational cells are indexed consecutively by three indices: $i = 1$ in the x-direction, $i = 2$ in the y-direction and $i = 3$ in the z-direction. Application of Eq. (1) over a computational cell, the changes in F in a cell reduce fluxes of F across the cell faces. The employed VOF method uses a type of donor-acceptor flux approximation δF downstream and upstream of a flux boundary that establishes an interface shape to use in computing the flux (see Hirt and Nichols [26] for more details on VOF).

A turbulent flow can be expressed by the instantaneous velocity u_i as the sum of a mean $U_i = \sqrt{u^2 + v^2 + w^2}$, and a fluctuating part u_i', as follows:

$$u_i = U_i + u_i' \tag{2}$$

Therefore, the Reynolds averaged equations of motion in conservation form are presented as follows:

$$\frac{\partial U_i}{\partial x_i} = 0 \tag{3}$$

$$\rho \frac{\partial U_i}{\partial_t} + \rho U_j \frac{\partial U_i}{\partial x_i} = \frac{-\partial P}{\partial x_i} + \frac{\partial}{\partial x_i}\left(2\mu S_{ji} - \rho\overline{u_j' u_i'}\right) \tag{4}$$

where u_i and x_i are velocity and position, t is time, p is pressure, ρ is water density, μ is the dynamic viscosity, and noting that $S_{ji} = S_{ij}$ is the strain-rate tensor defined by:

$$S_{ij} = \frac{1}{2}\left(\frac{\partial u_i}{\partial x_j} + \frac{\partial u_j}{\partial x_i}\right) \tag{5}$$

The value of $-\rho\overline{u_j' u_i'}$ is the Reynolds-stress tensor and we denote it by $\rho\ \tau_{ij}$, while τ_{ij} is the specific Reynolds stress tensor given by:

$$\tau_{ij} = -\rho\overline{u_j' u_i'} \tag{6}$$

where $\tau_{ij} = \tau_{ji}$.

2.4 Turbulence Models

Among the best-known turbulence models, there is the k-ε model [29], which is defined by a pair of transport equations for the turbulent kinetic energy k, and its dissipation ε. Over the years, this model has made it possible to approximate significant types of flows, although it is necessary to modify the dimensionless parameters. The k-ω model [30, 31] which is the most suitable for modeling free surface flows with streamwise pressure gradients like spreading jets, wakes, and plumes which are confirmed by Vanneste and Troch [23], Kurdistani *et al.,* [25], and Devolder *et al.,* [32] as well. A definitely cutting-edge model is the Re-Normalization-Group model (RNG) presented by Yakhot and Orszag [30] which is an appropriate model for estimating the transport coefficients in the advection of a passive scalar by incompressible turbulence. Overall, it can be said that the RNG method is more suitable for describing turbulent flows at reduced speed.

For the present study, a split Lagrangian advection method is used together with the RNG turbulence model (see Yakhot and Orszag [33]). The latter consists of four phases:

i. Rough fluid interface in a cell with a flat surface;
ii. Displacement of the fluid volume according to the local velocity range;
iii. Calculation of the new fluid fraction values in the cells using an overlay procedure.
iv. The sea condition consists of a constant current without considering the tidal effects

2.5 Advection Model

This section describes a model for the advection of the substances in fluids and tracking the solute. The dissolution of substances increases the density of the fluid and thus may affect the flow. The model accounts for the basic physical phenomena, such as mass transfer at the interface between solid and fluid, diffusion and convection of the dissolved solute in fluid, and, finally, the change in fluid density, viscosity, and surface tension coefficient [34, 35].

In Cartesian coordinates the advection operator is:

$$u.\nabla = u_x \frac{\partial}{\partial x} + u_y \frac{\partial}{\partial y} + u_z \frac{\partial}{\partial z} \tag{7}$$

Where $u = (u_x, u_y, u_z)$ is the velocity field and ∇ is the *nabla* operator. The amount of dissolved solute in a fluid is represented by its mass concentration C. The transport equation for C is:

$$\frac{\partial C}{\partial t} = (u.\nabla)C \tag{8}$$

The fluid mixture density ρ is assumed to be a linear function of concentration [36, 37]:

$$\rho = \rho_0 + \alpha\, C \tag{9}$$

Where ρ_0 is the density of pure liquid and α is a constant obtained experimentally. Accordingly, the fluid volume varies with the concentration, also linearly:

$$V = V_0\,[1 + (1 - \alpha)(C/\,\rho_0)] \tag{10}$$

The mixture density coefficient α may take values in the range between $1 - (\rho_{s/}\ \rho_0)$ for substitutional solutes (ρ_s is the substance density), when the solvent molecules are completely displaced by the larger molecules of the solute, and α =1 for interstitial solutes, when the smaller solute molecules fit perfectly in the spaces between the molecules of the solvent. It has to be noted that there is no change to the mixture volume upon dissolution when α = 1. This assumption can also be used as a simplification of the model if:

i. The velocity of the interface controlled by the dissolution rate is small compared to the average fluid velocity;
ii. The solute concentrations are small compared to fluid density.
iii. These assumptions are considered for the current study and α = 1.

2.6 Dimensional Analysis

Diffusion of the surface marine sewage effluent is a complex phenomenon and the mixing length scale can be thought of as a characteristic eddy size since such scales are different for each effluent flow and sea conditions, this phenomenon includes turbulence models that do not provide a length scale, and are incomplete (Wilcox [30]; Kurdistani *et al.,* [25]). To this end, we must know well something more about the effluent flow characteristics and sea conditions, than initial and boundary conditions, in advance in order to obtain a solution. Self-similarity which means reproducing itself on

different time and space scales is the right solution to reduce a problem in the mathematical physics of a phenomenon that generally leads to a power-law relationship confirmed in previous studies by several authors [38-42].

Generally, a power-law form of a function $f(x)$ appears in mathematical modeling of various phenomena in engineering in the form of $f(x) = a\, x_1^b\, x_2^c \ldots x_n^z$, where a, b, c, and z are constants. Self-similar solutions always limit problems in which the governing variables are either equal to zero or infinity. According to Tomasicchio *et al.,* [43], Tomasicchio and Kurdistani [44], and Kurdistani *et al.,* [45], significant importance is the analysis of *incomplete self-similarity* in fluid dynamics, for which solving a complete mathematical formulation of the problem is very difficult and sometimes impossible; therefore, the comparison of similarity laws with experimental or numerical data extremely depends on estimating the character of the self-similarity. A dimensional analysis has been conducted by using the Buckingham π-theorem [38, 46], in which it is assumed that the main parameters to determine the maximum intrusion length L_X are:

$$f(\rho, \rho_{sea}, C, U_{sea}, g, U_{jet}, L_X, h) = 0 \tag{11}$$

where f = functional symbol; h = water depth; ρ_{sea} = sea saltwater density; ρ = effluent water density; g = gravitational acceleration; C = effluent concentration; U_{jet} = effluent jet velocity; U_{sea} = sea current velocity; L_X = maximum intrusion length. According to the Buckingham π-theorem [24, 32], Eq. (11) can be expressed by the following non-dimensional parameters:

$$\Pi_1 = f(\Pi_2, \Pi_3, \Pi_4, \Pi_5) \tag{12}$$

The objective variable L_X has been normalized dividing by the total water depth h as the first non-dimensional parameter:

$$\Pi_1 = L_X / h \tag{13}$$

Following the Buckingham theorem, the next four dimensionless parameters were obtained:

$$\Pi_2 = \rho_{sea} / \rho \tag{14}$$

$$\Pi_3 = C / \rho \tag{15}$$

$$\Pi_4 = u_{sea} / (gh)^{0.5} = \mathrm{Fr}_{sea} \quad \text{(sea current Froude number)} \tag{16}$$

$$\Pi_5 = u_{jet} / (gh)^{0.5} = \mathrm{Fr}_{jet} \quad \text{(effluent jet Froude number)} \tag{17}$$

Therefore:

$$\frac{L_X}{h} = \varphi\left(\frac{\rho_{sea}}{\rho}, \frac{C}{\rho}, Fr_{sea}, Fr_{jet}\right) \tag{18}$$

Finally, Eq. 18 can be shown in a power-law expression as follows:

$$\frac{L_X}{h} = a\left(\frac{\rho_{sea}}{\rho}\right)^b \left(\frac{C}{\rho}\right)^c (1 + Fr_{sea})^d \left(1 + Fr_{jet}\right)^e \tag{19}$$

where *a*, *b*, *c*, *d*, and *e* are constants to be obtained experimentally.

2.7 Case Study for CFD Model

The coastal zone of Nardò in the Apulia region in the south of Italy includes a sea with crystalline nuances with shallow and transparent waters suitable for snorkeling, that varies between white sandy beaches, limestone esplanades, rock spurs, and ravines. This beautiful coast which is almost an all-season touristic coast has been considered as a protected marine natural area since 1997 to protect the precious natural heritage of the area. One of the most important issues to be considered in this matter is the wastewater discharge into the sea.

Although the discharged wastewater is already purified, always there is high environmental attention regarding this marine sewage because the protected marine area is only about 130 meters north of the effluent outlet. Therefore, the surface effluent of the purifier of the city Nardò has been selected as the case study for the numerical simulations (Figure 1). This purifier discharges 4500 m^3/day = 0.052 m^3/s and in the future because of the population growth will increase to 5000 m^3/day = 0.058 m^3/s. Therefore, for the experimental setup, these two effluent discharges have been considered plus an extreme effluent discharge Q = 0.1 m^3/s. These values of the wastewater discharge help to understand the effect of the quantity of the discharged wastewater when there is a small increase and when there is an extreme increase.

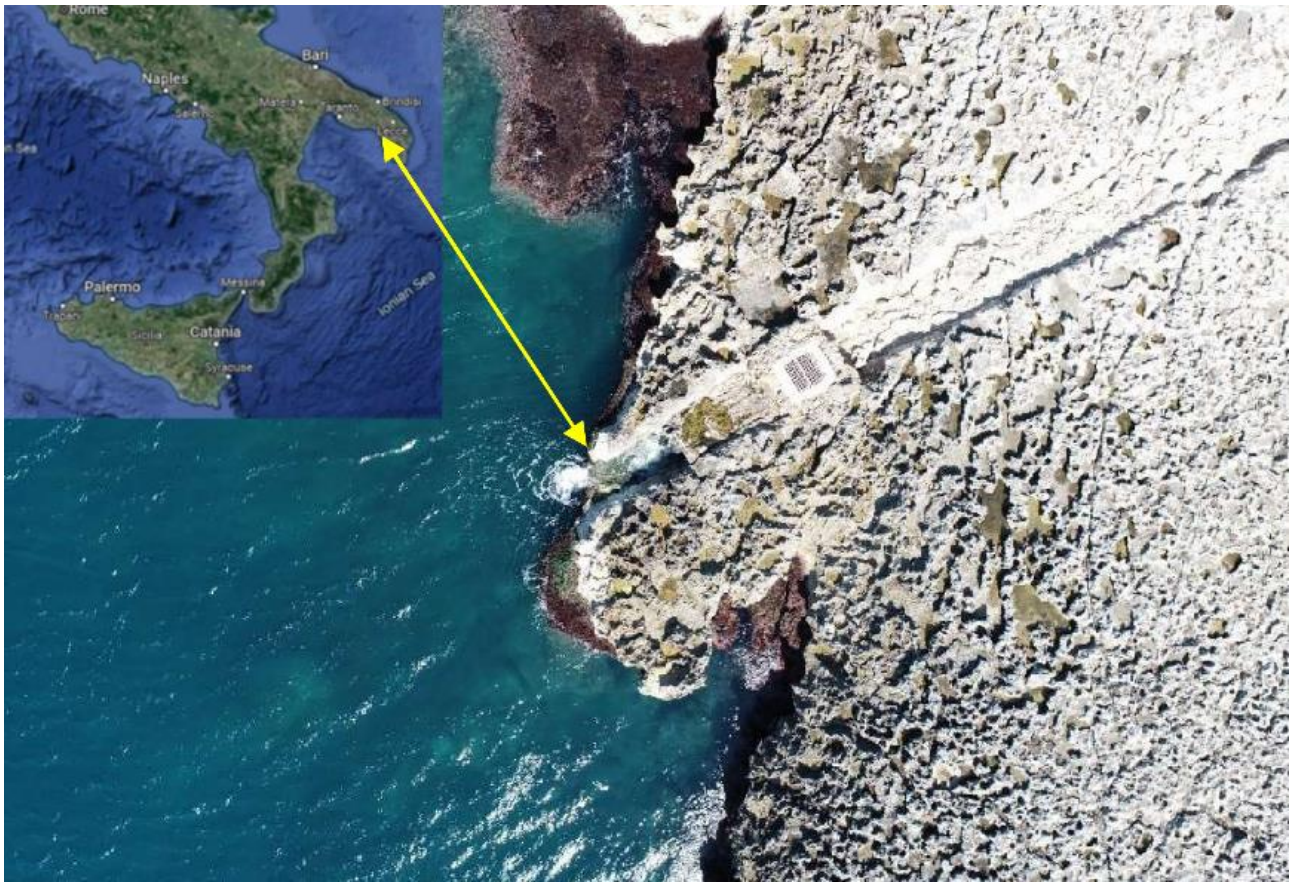

Fig. 1. The surface effluent of Nardò in the south of Italy

As it has been explained in dimensional analysis, the sea condition includes a constant current in no-tidal conditions. Therefore, a 3D Cartesian mesh has been prepared in the same geographic coordinates of the surface effluent of Nardò in the south of Italy (Figure 2). As it appears, any cell of

the calculation mesh has dimensions Δx = 2 m, Δy = 2.5 m, and Δz = 0.5 m that creates a mesh with a sum of 96000 cells. The position of the effluent on the real bathymetry (0.5 m × 0.5 m) inside the numerical mesh has been shown in Figure 3.

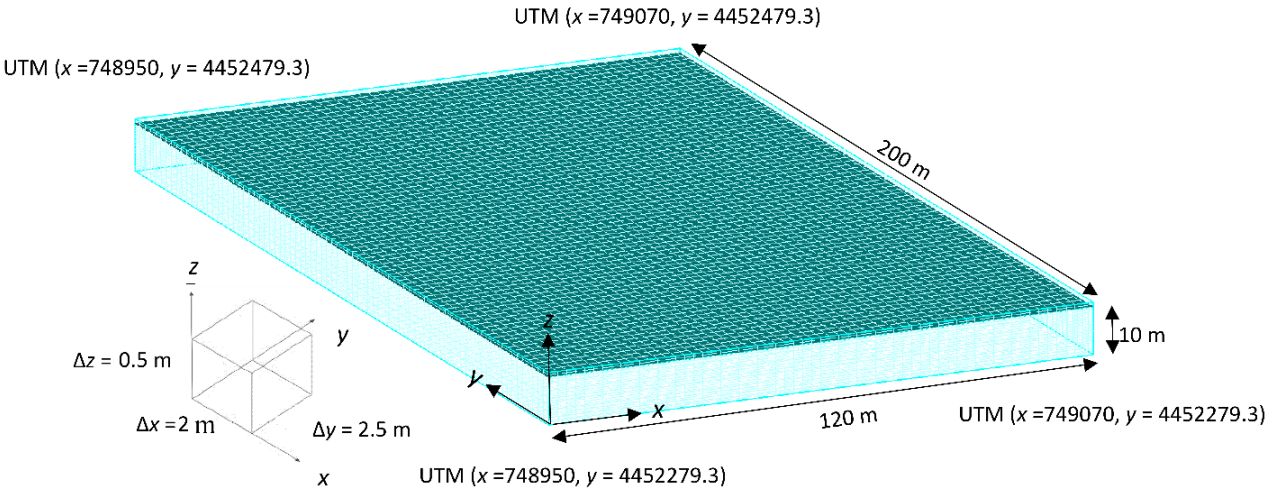

Fig. 2. Numerical mesh in UTM-WGS 84 system

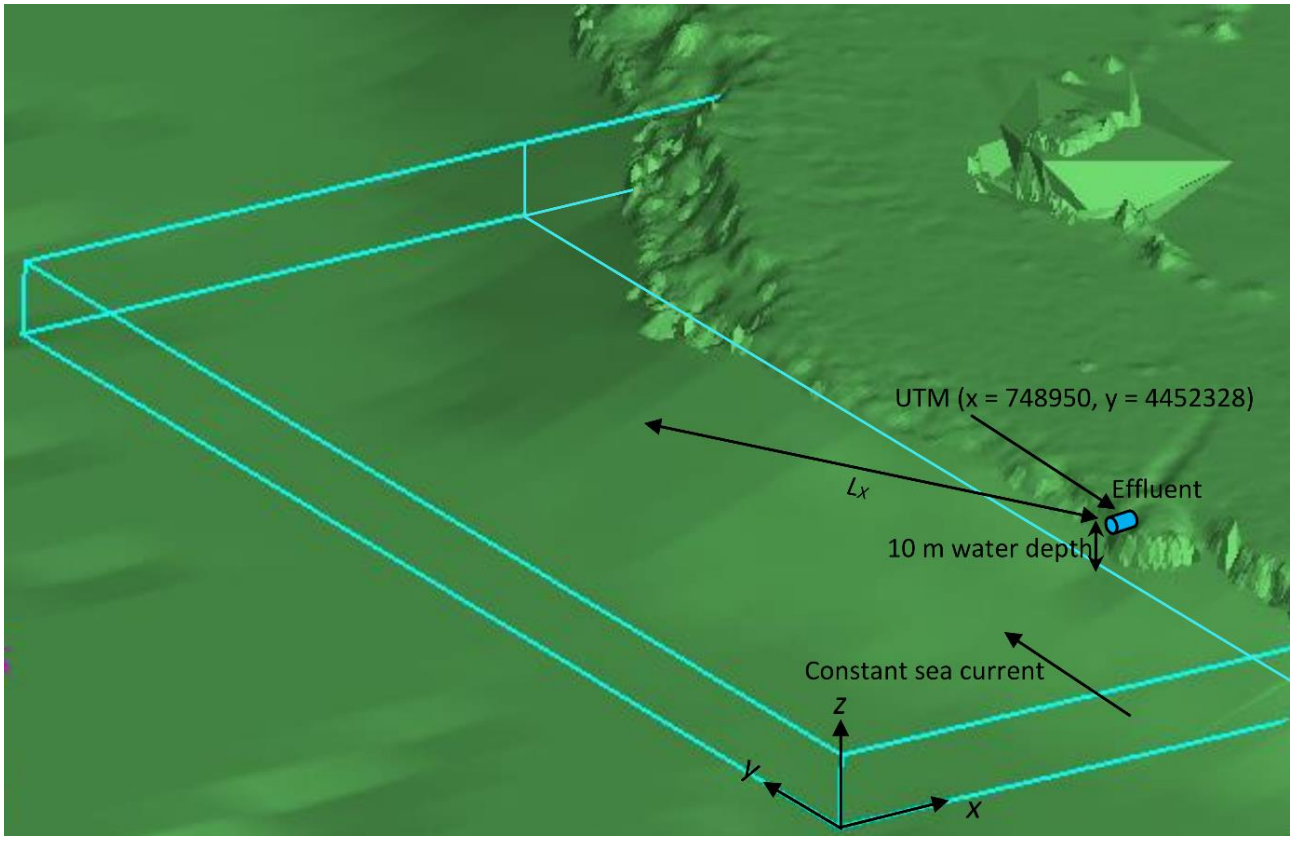

Fig. 3. The position of the effluent on the real bathymetry (0.5 m × 0.5 m) inside the numerical mesh in UTM-WGS 84 system

3. Results

3.1 Stability of the CFD Model

It is very important to have a stable numerical model before starting the diffusion of the effluent. Hence, the accuracy of the CFD model at the boundaries has been investigated. As it appears in Figure 3, the constant current velocity as the input boundary at the zero point of the *y*-axis and an outflow along with a constant water depth h = 10 m at the higher point of the *y*-axis are presented as the boundary condition to simulate a constant sea current along the coast in the *y* direction. The initial condition consists of a constant zero sea water level in no-tidal conditions.

The first parameter to be controlled is the current velocity at the upstream boundary of the calculation mesh. For this test, U_{sea} = 0.2 m/s in the *y*-axis direction has been used to see the model accuracy. Figure 4 shows the variation of the sea surface current velocity with respect to the constant velocity 0.2 m/s after 6 minutes of simulation in which the values of *x* of the UTM coordinates represent the z-y face of the mesh at *y* = 4452281, perpendicular to the current direction in the *y*-axis. The root means square error shows the 5.47% of deviation from the constant velocity of 0.2 m/s which is the result of the turbulent flow.

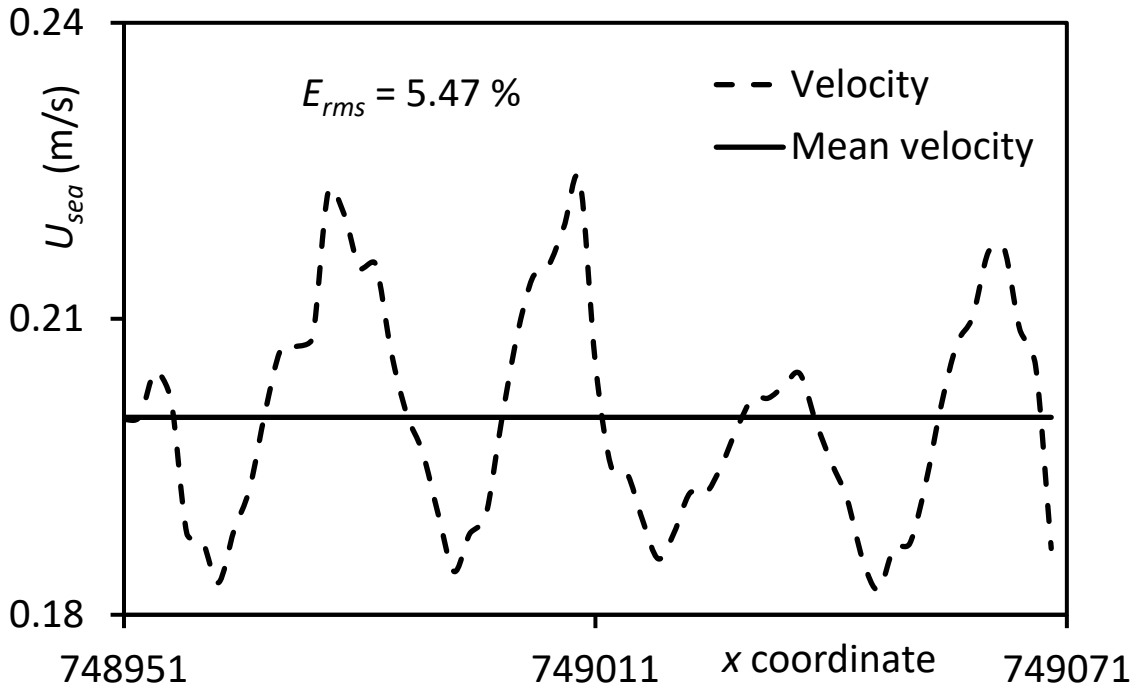

Fig. 4. The velocity variations at the upper boundary of the numerical mesh after 6 minutes of simulation (x coordinates are in UTM-WGS 84 system)

To show the stability of the CFD model, the velocity variations at the upper boundary of the numerical mesh after 60 minutes of simulation are shown in Figure 5 showing the effect of turbulent flow and 4.79% deviation from the constant velocity of 0.2 m/s.

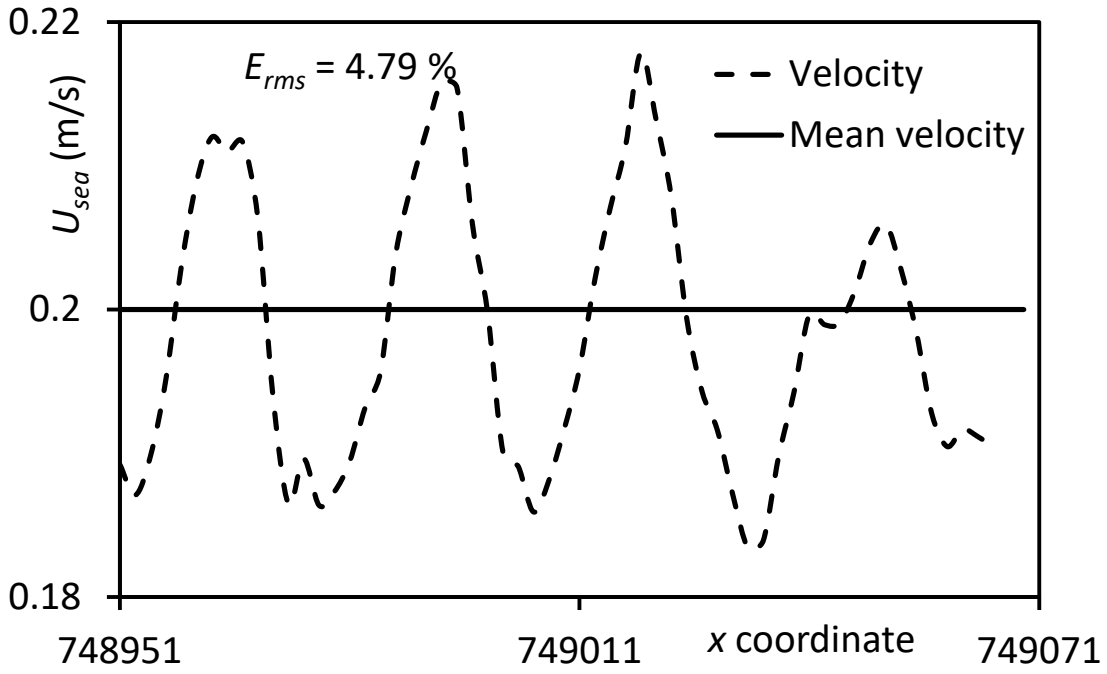

Fig. 5. The velocity variations at the upper boundary of the numerical mesh after 60 minutes of simulation (x coordinates are in UTM-WGS 84 system)

The second parameter to be checked is the water depth at the lower boundary of the numerical mesh at a higher point of the *y*-axis. Figure 6 shows the water depth variations after 6 minutes of simulation in which the values of *x* coordinates represent the z-y face of the mesh at *y* = 4452478, perpendicular to the current direction in the y-axis. The root means square error shows the 0.1% of deviation from the mean water depth *h* = 10 m. Figure 7 shows the stability of the numerical model presenting only a 0.3% of deviation from the mean water depth at the lower boundary of the numerical mesh after 60 minutes of simulation.

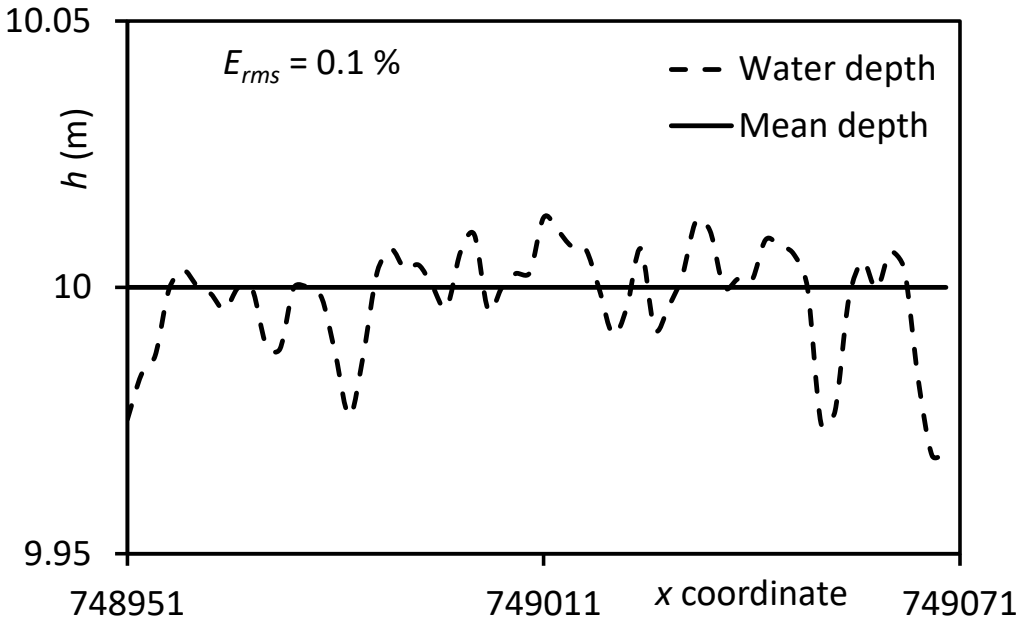

Fig. 6. The water depth variations at the lower boundary of the numerical mesh after 6 minutes of simulation (x coordinates are in UTM-WGS 84 system)

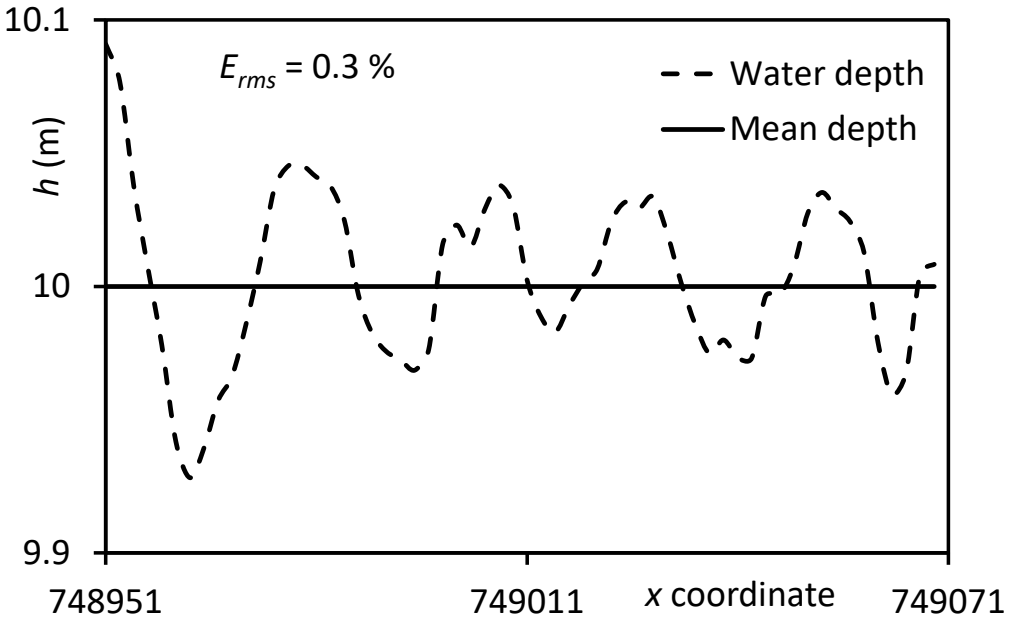

Fig. 7. The water depth variations at the lower boundary of the numerical mesh after 60 minutes of simulation (x coordinates are in UTM-WGS 84 system)

3.2 Numerical Tests

To find the mathematic form of Eq. (19) it is needed to provide a big dataset conducting laboratory tests or field measurements in which due to the experimental setup limitations and expensive and time-consuming field measurement data acquisition, it has been decided to use a CFD model to make numerical experiments for different combinations of the parameters mentioned in Eq. (19) for different effluent discharges and concentrations and different sea conditions. Finally, a formula is proposed to predict the maximum length of the effluent intrusion that the scalar losses 95% of its concentration.

The effluent is discharged to the sea through a conduit in 1 m diameter with a free flow velocity U_{jet}. As it appears from Table 1, three different effluent discharges Q = 0.052, 0.058, and 0.1 m^3/s have been considered for simulations in which in consequence U_{jet} = 0.245, 0.251, and 0.291 m/s. The sea salt-water density has been considered for two extreme conditions; winter with the highest density ρ_{sea} = 1033 Kg/m^3, and summer with the lowest density ρ_{sea} = 1022.4 Kg/m^3 [20]. Three different scalar concentrations have been tested C = 0.5, 1, and 2 Kg/m^3. A wide range of the sea surface current velocity ($0.01 \leq U_{sea} \leq 0.5$ m/s) has been tested. Both Froude numbers for the sea current and effluent velocity are determined for a seawater depth of h = 10 m.

All the maximum intrusion length values (L_X) presented in the last column of Table 1 are extracted from the results of Flow-3D simulations after 7 hours of duration. Figure 8 shows the time-evolution of the scalar intrusion during 7 hours of simulation (test. No. 3 of Table 1) showing clearly that the length of the scalar intrusion after one hour (Figure 8(a)) reaches the maximum value that the scalar concentration diminishes to 5% with respect to the initial concentration and practically during other 6 hours of the simulation, there is not any significant increase in the value of the maximum intrusion length (L_X). The counter lines are used to show better the time evolution of the scalar length intrusion.

Table 1
Experimental range

Test	Q (m³/s)	ρ_{sea} (Kg/m³)	C (Kg/m³)	U_{sea} (m/s)	U_{jet} (m/s)	Fr_{sea}	Fr_{jet}	W (m)	L_X (m)
1	0.058	1022.4	1.0	0.010	0.251	0.0010	0.0254	6.30	46.0
2	0.052	1022.4	0.5	0.010	0.245	0.0010	0.0248	5.30	37.4
3	0.052	1022.4	1.0	0.050	0.245	0.0050	0.0248	6.10	42.8
4	0.058	1022.4	1.0	0.050	0.251	0.0050	0.0254	6.00	42.8
5	0.052	1022.4	1.0	0.500	0.245	0.0505	0.0248	0.46	3.2
6	0.052	1022.4	1.0	0.100	0.245	0.0101	0.0248	2.50	19.3
7	0.052	1022.4	2.0	0.500	0.245	0.0505	0.0248	0.45	3.2
8	0.052	1022.4	2.0	0.100	0.245	0.0101	0.0248	2.97	21.4
9	0.100	1022.4	2.0	0.500	0.291	0.0505	0.0294	1.43	10.7
10	0.100	1022.4	2.0	0.100	0.291	0.0101	0.0294	4.90	35.3
11	0.100	1022.4	0.5	0.100	0.291	0.0101	0.0294	4.72	34.0
12	0.052	1022.4	0.5	0.050	0.245	0.0050	0.0248	4.70	35.3
13	0.100	1033.0	0.5	0.100	0.291	0.0101	0.0294	4.21	29.9
14	0.100	1033.0	2.0	0.100	0.291	0.0101	0.0294	4.01	28.9
15	0.052	1033.0	1.0	0.100	0.245	0.0101	0.0248	2.28	17.1
16	0.052	1033.0	1.0	0.050	0.245	0.0050	0.0248	4.35	30.0
17	0.052	1033.0	1.0	0.020	0.245	0.0020	0.0248	4.57	32.0
18	0.052	1022.4	1.0	0.020	0.245	0.0020	0.0248	5.05	37.4
19	0.052	1022.4	0.5	0.020	0.245	0.0020	0.0248	4.89	34.2
20	0.058	1022.4	1.0	0.020	0.251	0.0020	0.0254	5.64	40.6
21	0.100	1033.0	2.0	0.050	0.291	0.0050	0.0294	4.68	34.2
22	0.100	1022.4	1.0	0.500	0.291	0.0505	0.0294	1.55	10.7
23	0.100	1022.4	1.0	0.100	0.291	0.0101	0.0294	4.89	33.2
24	0.100	1022.4	1.0	0.050	0.291	0.0050	0.0294	6.39	46.0
25	0.100	1022.4	1.0	0.010	0.291	0.0010	0.0294	7.28	54.6
26	0.052	1022.4	1.0	0.300	0.245	0.0303	0.0248	1.71	11.8
27	0.052	1022.4	1.0	0.200	0.245	0.0202	0.0248	2.01	13.9

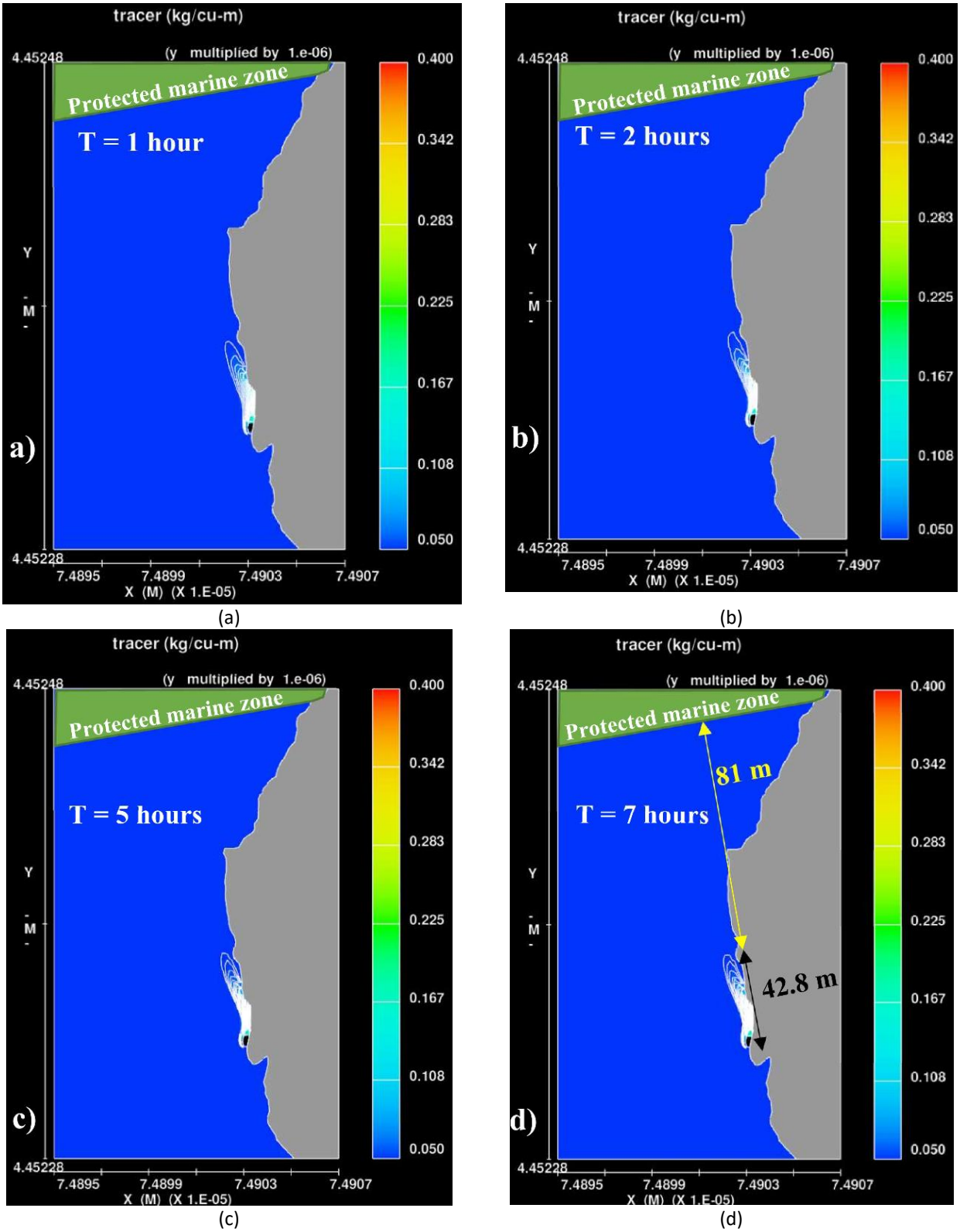

Fig. 8. Time-evolution of the scalar intrusion during 7 hours of simulation (test. No. 3 of Table 1); Q = 0.058 m^3/s, ρ_{sea} = 1022.4 Kg/m^3, C = 1.0 Kg/m^3, U_{sea} = 0.050 m/s, U_{jet} = 0.251 m/s (x and y coordinates are in UTM-WGS 84 system) at a) T=1 hour, b) T=2 hour, c) T=5 hour, and d) T=7 hour

Figure 8 shows the protected marine zone about 130 meters north of the effluent outlet in which the historical observations do not show any scalar concentration arriving at the protected marine

zone. As it is shown in Table 1, this is approved by a set of numerical tests that in the worst case, the maximum length of the scalar intrusion is less than 60 meters.

3.3 Validation of the CFD Model

Kim and Cho [18] calibrated a CFD-RANS model (Flow-3D) to simulate the buoyant flow of surface-heated water discharged in shallow water and verified the accuracy of the numerical results using the hydraulic experimental data adapted from McGurik and Rodi [19]. They defined a recirculation zone in the length of *L* and width of *W* that is shown in a plan view in Figure 9.

Kim and Cho [13] experimentally presented the ratio $L_x/W \approx 7$ to 7.5. The maximum length of the effluent intrusion X = 42.8 m presented in Figure 8(d) happened in a width of W = 6 m that means L_x/W = 7.1 which is in the range of the calibrated Flow-3D model by Kim and Cho [18] that is shown in Figure 10.

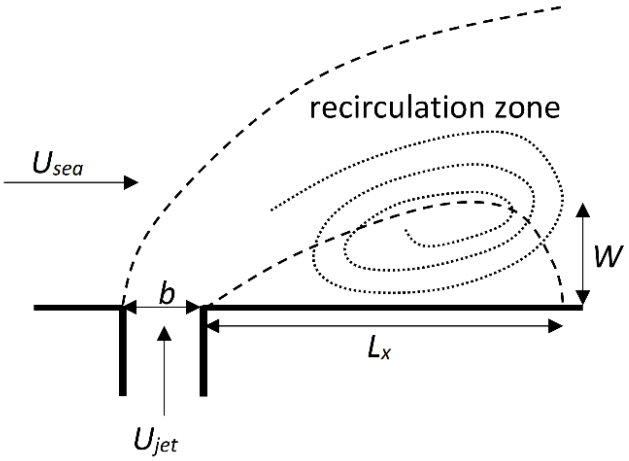

Fig. 9. Plan view of the recirculation zone in a thermal surface side discharge

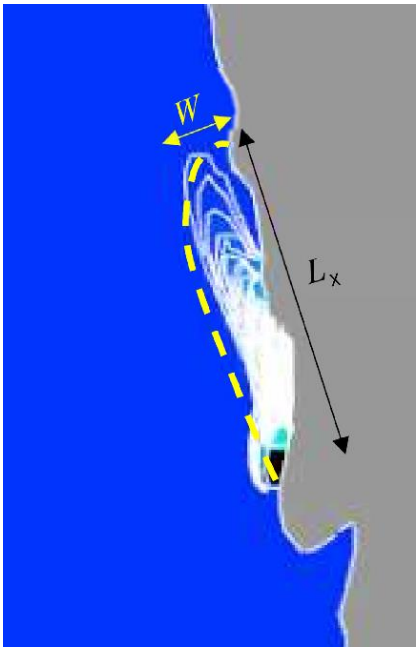

Fig. 10. A close-up of the plan view of the recirculation zone for Exp. No. 3 of Table 1

Looking at *W* values presented in Table 1 depicts that for all 27 experiments, the range of $L_x/W \approx$ 7 to 7.5 has been observed confirming the results from Kim and Cho [18]. This means that the CFD model is validated regarding the heat transfer module of the model. Therefore, the CFD model is able to simulate the density exchange between effluent and seawater in a stable mode.

3.4 Proposed Formula

A variables sensitivity test shows that the normalized scalar intrusion length L_X/h is directly a function of Fr_{sea} showing a power form trend where increasing Fr_{sea}, decreases L_X/h. Therefore, as it is shown in Figure 11, Fr_{sea} is considered a self-similarity character that can represent the main trend of the phenomenon independent of the other parameters.

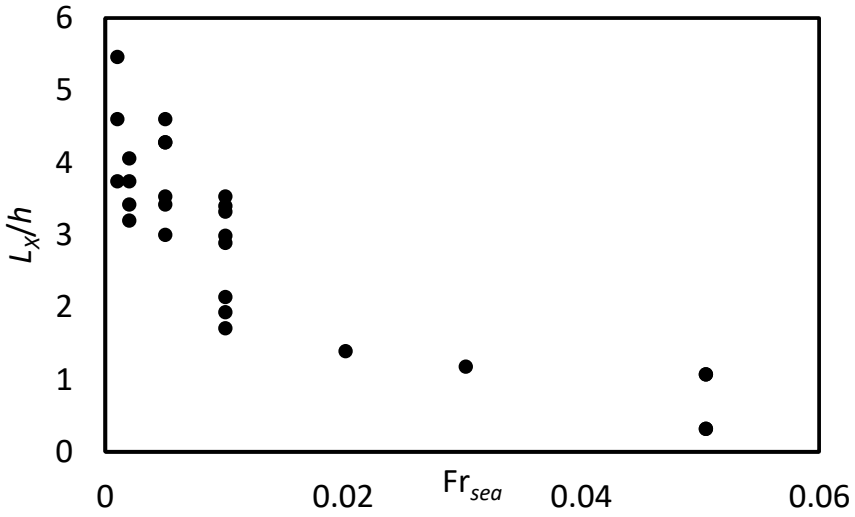

Fig. 11. L_X/h as a function of Fr_{sea}

Application of a multivariate regression on results from Flow-3D simulations (the L_X column in Table 1) leads to a power-law formula to determine the maximum length of the effluent intrusion that scalar losses 95% of its concentration as follows (R^2 = 0.92):

$$\frac{L_X}{h} = 1.64\left(\frac{\rho_{sea}}{\rho}\right)^{-21.9}\left(\frac{C}{\rho}\right)^{-0.017}(1+Fr_{sea})^{-47.9}\left(1+Fr_{jet}\right)^{64} \quad (20)$$

The results from the CFD model are compared with the results from Eq. (20) in Figure 12 showing a good agreement within 20% of deviation from the perfect agreement line.

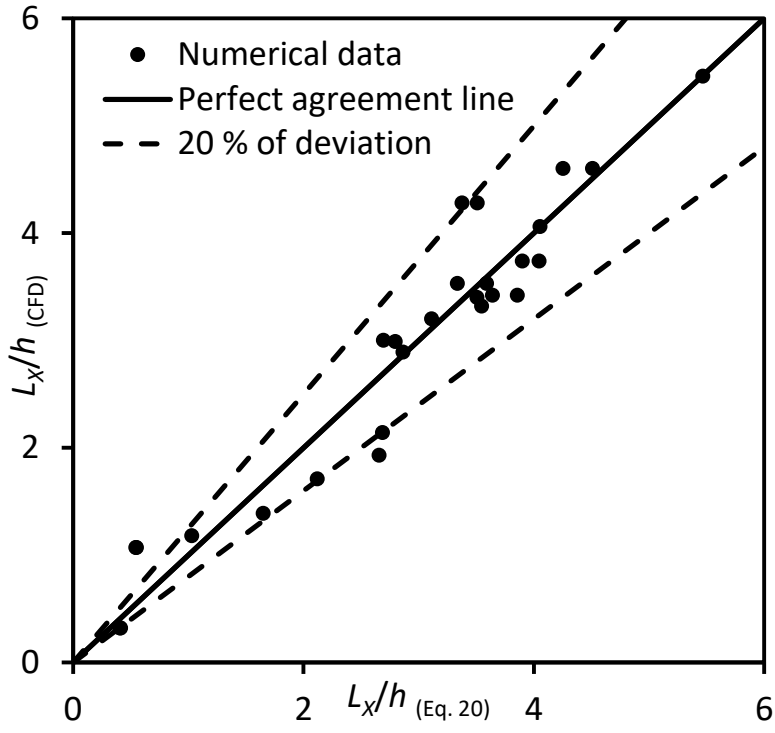

Fig. 12. The comparison of the CFD model results with the predicted L_X values by Eq. (20)

4. Discussion

Mikhail *et al.,* [47] have measured the width and length of the recirculation eddy in an open-channel flow situation. From dimensional analysis, they concluded that the shape of the eddy is unaffected by the width ratio b/B and that the size of the eddy depends mainly on the momentum flux ratio $M = (U_{jet}/U_{canal})^2(b/B)$ where B is the channel width. In the current study as the jet discharges to the sea, instead of the channel width B, the width of the recirculation zone W is substituted and, in consequence, instead of U_{canal}, the sea current mean velocity U_{sea} is used to determine the momentum flux ratio M as follows:

$$M = \left(\frac{U_{jet}}{U_{sea}}\right)^2 \left(\frac{b}{W}\right) \tag{21}$$

Figure 13 compares the non-dimensional ratio of W/L_X with the momentum flux ratio M. It shows a good accordance between data from Mikhail *et al.,* [47] and the current study CFD results that approves the results from the newly proposed Eq. (20). All results confirm that W/L_X remains almost constant ($0.1 \geq W/L_X \geq 0.2$) with increasing the momentum flux ratio M. In other words, by increasing the length of the scalar intrusion, the width of the recirculation zone W will increase as well in such a way that the ratio W/L_X remains constant.

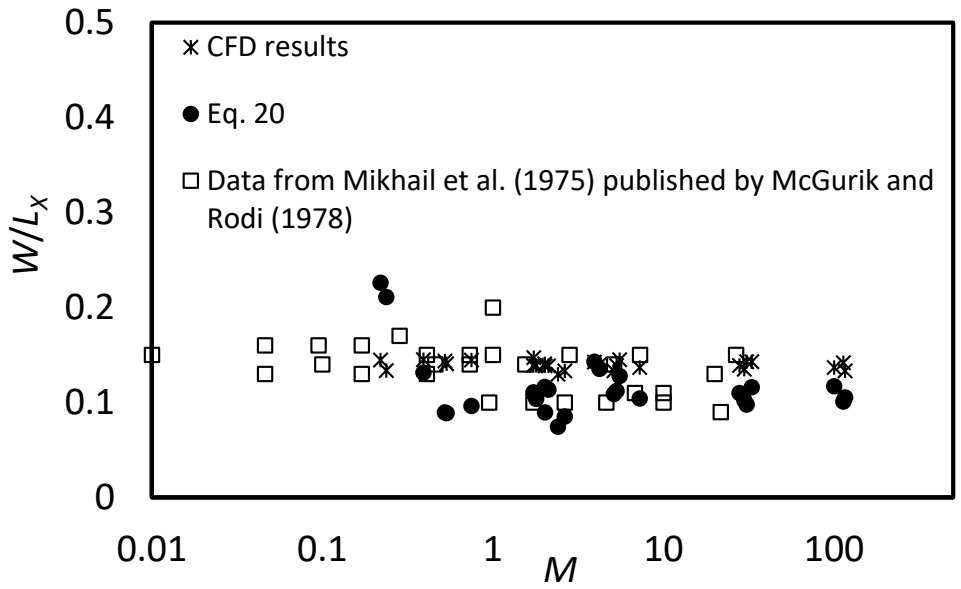

Fig. 13. The comparison of the CFD model results with the predicted L_X values by Eq. (20)

5. Conclusions

A formula is proposed to predict the maximum length of effluent intrusion at surface marine sewage. A series of numerical experiments have been performed, after an appropriate stability test of the CFD model. Application of incomplete self-similarity showed that the length of a surface marine effluent intrusion is a direct function of the sea current Froude number that is considered the self-similarity character for the surface marine effluent diffusion. Increasing the sea current Froude number decreases the length of the effluent intrusion. Dimensional analysis depicted that besides the sea current Froude number, the sea saltwater density, the scalar concentration, and the effluent jet Froude number are the main important parameters to be considered in the prediction of the

surface marine effluent intrusion length. The application of a multivariate regression led to a power form formula to predict the length of a surface marine effluent intrusion. Results showed that increasing the ratio of the seawater density to the freshwater density and increasing the seawater Froude number diminishes the maximum length of the effluent intrusion (losing 95% of the effluent concentration on the sea surface). The proposed formula helps engineers to predict rapidly the maximum length of the sea surface effluent intrusion without conducting any numerical simulation giving them an initial idea to make a decision especially when the discharged effluent may arrive at a marine protected zone.

Acknowledgement
The authors would like to express their gratitude and sincere appreciation to the anonymous reviewers for their useful comments and suggestions for improving this work.

References

[1] Rawn, A.M., Bowerman, F.R., and Brooks, N.H. "Diffusers for Disposal of Sewage in Sea Water." *J. Sanitary Eng. Div. ASCE.* 86 no. SA2 (1959): 65–105. https://doi.org/10.1061/JSEDAI.0000274

[2] Chow, M.M., Cardoso, S.S.S., and Holford, J.M. "Dispersion of Pollutants Discharged into the Ocean, The Interaction of Small- and Large-scale Phenomena." *Trans IChemE, Part A, Chemical Engineering Research and Design*, 82 no. A6 (2004): 730–736. https://doi.org/10.1205/026387604774196019

[3] Kim, Y.D., Seo, I.W., Kang, S.W., and Oh, B.C. "Modeling the Mixing of Wastewater Effluent Discharged from Ocean Outfalls using a Hybrid Model." *Coastal Engineering Journal*, 43 no. 4 (2001): 259-288. https://doi.org/10.1142/S0578563401000372

[4] Bricker, J.D., and Nakayama, A., "Estimation of far-field horizontal and vertical turbulent diffusion coefficients from the concentration field of a wastewater plume near the Akashi Strait." *Environ. Fluid Mech*. 7 (2007): 1–22. https://doi.org/10.1007/s10652-006-9013-4

[5] Zhao, L., Chen, Z., and Lee, K. "Modelling the dispersion of wastewater discharges from offshore outfalls: a review." *Environ. Rev.* 19 (2011): 107–120. https://doi.org/10.1139/a10-025

[6] Inan, A. "Modeling of Hydrodynamics and Dilution in Coastal Waters." *Water*. 11 no. 83 (2019): https://doi.org/10.3390/w11010083

[7] Wang, C., Guo, Z., Li, Q., and Fang, J. "Study on layout optimization of sewage outfalls: a case study of wastewater treatment plants in Xiamen." *Scientific Reports*, 11 (2021):18326, https://doi.org/10.1038/s41598-021-97756-9

[8] Ho, M., Molemaker, J.M., Kessouri, F., McWilliams, J.C., and Gallien, T.W. "High-Resolution Nonhydrostatic Outfall Plume Modeling: Cross-Flow Validation" *Journal of Hydraulic Engineering*. 147 no. 8 (2021): 04021028. 10.1061/(ASCE)HY.1943-7900.0001896

[9] Panseriya, H.Z. Gosai, H.B. Gavali, D.J. and Dave, B.P. "Assessment of surface water quality during different tides and an anthropogenic impact on coastal water at Gulf of Kachchh, West Coast of India" *Environmental Science and Pollution Research*. 30 no. 10 (2023): 28053 – 28065. 10.1007/s11356-022-24205-z

[10] Santavy, D.L. Horstmann, C.L., Huertas, E., and Raimondo, S. "Comparison of coral reef communities in proximity to ocean effluent pipes off the north coast of Puerto Rico" *Environmental Monitoring and Assessment*. 195 no. 1 (2023): 162. 10.1007/s10661-022-10756-8

[11] Brooks, N. H. "Diffusion of sewage effluent in an ocean-current." *In Proc. 1st Int. Conf. on Waste Disposal in the Marine Environment*. University of California, Berkeley, (1959): 246-267. https://doi.org/10.1016/B978-0-08-009534-9.50018-1

[12] Bennet, N. J. "Design of Sea Outfalls the Lower Limit Concept of Initial Dilution." *In Proc. Instn Ciu. Engrs*., 75 (1983):113–121. https://doi.org/10.1680/iicep.1983.1391

[13] Sharp, J. J. "Marine outfalls for small coastal communities in Atlantic Canada." *Can. J. Civ. Eng.*, 18 (1991): 388-396. https://doi.org/10.1139/l91-049

[14] Caine, R. F. "Sea Outfalls for the Disposal and Treatment of Wastewater Effluents." *Wal. Sci. Tech*, 32 no. 7 (1995): 79–86. https://doi.org/10.1016/0273-1223(96)00050-9

[15] Matos, J., Monteiro, A., Costa, P., Neves, R., Bettencourt, A., Frazao, A., and Santos, C. "Wastewater Diffusion in the Estoril Coast: Theoretical Calculations and Field Studies." *Wal. Sci Tech*. 38 no. 10 (1998): 337-344. https://doi.org/10.1016/S0273-1223(98)00768-9

[16] Montaño-Ley, Y., Peraza-Vizcarra, R., and Páez-Osuna, F. "Tidal Hydrodynamics and their Implications for the Dispersion of Effluents in Mazatlán Harbor: An Urbanized Shallow Coastal Lagoon" *Water Air Soil Pollut.,* 194 (2008): 343–357. DOI 10.1007/s11270-008-9721-0

[17] Marques, G.M., Shao, A.E., Scott D. Bachman, S.D., Danabasoglu, G., and Bryan, F.O. "Representing Eddy Diffusion in the Surface Boundary Layer of Ocean Models with General Vertical Coordinates" *J. of Adv. in Model. Earth Sys.*, 15 no. 6 (2023): e2023MS003751. https://doi. org/10.1029/2023MS003751

[18] Kim, D. G., & Cho, H. Y. "Modeling the Buoyant Flow of Heated Water Discharged from Surface and Submerged Side Outfalls in Shallow and Deep Water with a Cross Flow." *Environ. Fluid Mech*. 6 (2006): 501–518. https://doi.org/10.1007/s10652-006-9006-3

[19] McGuirk, J. J., & Rodi, W. "A Depth-Averaged Mathematical Model for the Near Field of the Side Discharge into Open-Channel Flow." *J. Fluid Mech*. 86 no. 4 (1978): 761–781. https://doi.org/10.1017/S002211207800138X

[20] Dhanak, M.R., and Xiros, N.I. (Eds.) *Springer Handbook of Ocean Engineering*. Springer Dordrecht Heidelberg, London New York (2016). DOI 10.1007/978-3-319-16649-0

[21] Barkhudarov, M.R. "Lagrangian VOF advection Method for FLOW-3D" *Flow Science, Inc.* FSI-03-TN63-R (2004): 1–11. https://www.flow3d.co.kr/wp-content/uploads/FSI-03-TN63-R_lagrangian-vof.pdf

[22] Starobin, A., Hirt, T., Lang, H., & Todte, M. "Core drying simulation and validation." *Int. Found Res.* 64 no. 1 (2011): 1–5.

[23] Vanneste, D., and Troch, P. "2D Numerical Simulation of Large-Scale Physical Model Tests of Wave Interaction with a Rubble-Mound Breakwater." *Coast. Eng.* 103 (2015): 22–41. https://doi.org/10.1016/j.coastaleng.2015.05.008

[24] Kurdistani, S.M., Tomasicchio, G.R., Conte, D., and Mascetti, S. "Sensitivity Analysis of Existing Exponential Empirical Formulas for Pore Pressure Distribution Inside Breakwater Core Using Numerical Modeling." *special issue, Italian J. Eng. Geol. Environ.* 1 (2020): 65–71. https://doi.org/10.4408/IJEGE.2020-01.S-08

[25] Kurdistani, S.M., Tomasicchio, G.R., D'Alessandro, F., & Francone, A. "Formula for wave transmission at submerged homogeneous porous breakwaters." *Ocean Engineering*. 266 (2022): 113053. https://doi.org/10.1016/j.oceaneng.2022.113053

[26] Niknahad, A., and Bak Khoshnevis, A. "Numerical study and comparison of turbulent parameters of simple, triangular, and circular vortex generators equipped airfoil model" *J. of Adv. Res. in Num. Heat Trans.* 8 no. 1 (2022): 1–18.

[27] Hirt, C.W., and Nichols, B.D. "Volume of Fluid (VOF) Method for the Dynamics of Free Boundaries." J. *Comput. Phys*. 39 (1981): 201–225. https://doi.org/10.1016/0021-9991(81)90145-5

[28] Shehab, A., El-Baz, A.M.R., and Elmarhomy, A.M. "CFD Modeling of Regular and Irregular Waves Generated by Flap Type Wave Maker" *J. of Adv. Res. in Num. Heat Trans.* 85 no. 2 (2021): 128–144. https://doi.org/10.37934/arfmts.85.2.128144

[29] Harlow, F.H., and Nakayama, P.I. "Turbulence Transport Equations." *Phys. Fluids* 10 no. 11 (1967): 2323–2332. https://doi.org/10.1063/1.1762039

[30] Wilcox, D. C. (2006). Turbulence Modeling for CFD. DCW Industries Inc. San Diego. Third Edition.

[31] Wong, M.K., Sheng, L.C., Nor Azwadi, C.S., and Hashim, G.A. "Numerical Study of Turbulent Flow in Pipe with Sudden Expansion" *J. of Adv. Res. in Fluid Mech. and Thermal Sci.* 6 no. 1 (2015): 34–48.

[32] Devolder, B., Rauwoens, P., and Troch, P. "Application of a Buoyancy-Modified k-ω SST Turbulence Model to Simulate Wave Run-up Around a Monopile Subjected to Regular Waves using OpenFOAM." *Coast. Eng*. 125 (2017): 81–94. https://doi.org/10.1016/j.coastaleng.2017.04.004

[33] Yakhot, V., and Orszag, S.A. "Renormalization Group Analysis of Turbulence. I. Basic theory." *J. Sci. Comput*. 1 no. 1 (1986): 3–51. https://doi.org/10.1007/BF01061452

[34] Seager, R.J., Acevedo, A.J., Spill, F., and Zaman, M.H. "Solid dissolution in a fluid solvent is characterized by the interplay of surface area-dependent diffusion and physical fragmentation." *Scientific Reports*. No. 8:7711 (2018): 1-17. DOI:10.1038/s41598-018-25821-x

[35] Sahak, A.S.A., Nor Azwadi, C.S., Yusof, S.N.A., and Alamir, M.A. "Numerical Study of Particle Behaviour in a Mixed Convection Channel Flow with Cavity using Cubic Interpolation Pseudo-Particle Navier-Stokes Formulation Method" *J. of Adv. Res. in Num. Heat Trans.* 1 no. 1 (2020): 32–51.

[36] Sathishkumar, S., Rao, B.S., Pradeep, S., and Sairam R.M.S., Kalaiarasu, B., and Selvaraj, B. "Modelling and Validating the Spray Characteristics of a Co-axial Twin-Fluid Atomizer Using OpenFOAM" *J. of Adv. Res. in Fluid Mech. and Thermal Sci.* 91 no. 1 (2022): 35–45. https://doi.org/10.37934/arfmts.91.1.3545

[37] Nor Azwadi, C.S. and Adamu, I.M. "Turbulent Force Convective Heat Transfer of Hybrid Nano Fluid in a Circular Channel with Constant Heat Flux" *J. of Adv. Res. in Fluid Mech. and Thermal Sci.* 19 no. 1 (2016): 1–9.

[38] Barenblatt, G. I. (1987). *Dimensional Analysis*. Gordon and Breach Science Publishers. New York.

[39] Pagliara, S., Kurdistani, S.M., & Roshni, T. "Rooster tail wave hydraulics of chutes." *J. Hydraul. Eng. ASCE*. 137 no.9 (2011): 1085 – 1088. https://doi.org/10.1061/(ASCE)HY.1943-7900.0000397

[40] Pagliara, S., and Kurdistani, S.M. "Scour Characteristics Downstream of Grade-Control Structures." *In Proc. 7th Intl. Conf. on Fluvial Hydraulics-River Flow 2014.* Schleiss *et al*. (Eds). Lausanne. (2014): 2093-2098.

[41] Pagliara, S., Palermo, M., Kurdistani, S.M., and Hassanabadi, L. "Erosive and Hydrodynamic Processes Downstream of Low-Head Control Structures." *J. of Appl. Water Eng. and Res*. 3 no. 2 (2015): 122–131. https://doi.org/10.1080/23249676.2014.1001880

[42] Kurdistani, S.M., Tomasicchio, G.R., D'Alessandro, F., and Hassanabadi, L. "River Bank Protection from Ship-induced Waves and River Flow." *Water Sci. Eng*. 12 no. 2 (2019): 129–135. https://doi.org/10.1016/j.wse.2019.05.002

[43] Tomasicchio, G.R., Kurdistani, S.M., D'Alessandro, F., and Hassanabadi, L. "Simple Wave Breaking Depth Index Formula for Regular Waves." *J. Waterway. Port, Coast. Ocean Eng.* 146 no. 1 (2020): 06019001. https://doi.org/10.1061/(ASCE)WW.1943-5460.0000539

[44] Tomasicchio, G.R., & Kurdistani. S.M. "A New Prediction Formula for Pore Pressure Distribution inside Rubble Mound Breakwater Core." *J. Waterway. Port, Coast. Ocean Eng.* 146 no. 3 (2020): 04020005. https://doi.org/10.1061/(ASCE)WW.1943-5460.0000555

[45] Kurdistani, S.M., Aristodemo, F., Francone, A., Tripepi, G., and Tomasicchio, G.R. "Formula for the Maximum Reference Pressure at the Interface of the Breakwater Core and Filter Layer." *Coast Eng. J.* 63 no. 4 (2021): 532–544. https://doi.org/10.1080/21664250.2021.1982518

[46] Verri, G., Kurdistani, S.M., Coppini, G., and Valentini, A. "Recent Advances of a Box Model to Represent the Estuarine Dynamics: Time-Variable Estuary Length and Eddy Diffusivity." *J. Adv. Model. Earth Systems*. AGU 13 (2021): e2020MS002276. https://doi.org/10.1029/2020MS002276

[47] Mikhail, R., Chu, V.H., and Savages, S.B. "The reattachment of a two-dimensional turbulent jet in a confined cross flow." *Proc. 16th IAHR Cong*., Sao Paulo, Brazil, no. 3 (1975): 414-419.